Diverse RNA Structures Induce PRC2 Dimerization and Inhibit Histone Methyltransferase Activity

Jiarui Song[1,2,3], Liqi Yao[1], Anne R. Gooding[1,2,3], Valentin Thron[1,2,3], Vignesh Kasinath[1]* and Thomas R. Cech[1,2,3]*

[1]Department of Biochemistry, University of Colorado Boulder, Boulder, CO 80303, USA.

[2]BioFrontiers Institute, University of Colorado Boulder, Boulder, CO 80303, USA.

[3]Howard Hughes Medical Institute, University of Colorado Boulder, Boulder, CO 80303, USA.

*Corresponding author. Email: thomas.cech@colorado.edu (T.R.C.); vignesh@colorado.edu (V.K.)

SUMMARY

Methyltransferase PRC2 (Polycomb Repressive Complex 2) introduces histone H3K27 trimethylation, a repressive chromatin mark, to tune the differential expression of genes. PRC2 is precisely regulated by accessory proteins, histone post-translational modifications and, notably, RNA. Research on PRC2-associated RNA has mostly focused on the tight-binding G-quadruplex (G4) RNAs, which inhibit PRC2 enzymatic activity in vitro and in cells. Our recent cryo-EM structure provided a molecular mechanism for G4 RNA inactivating PRC2 via dimerization, but it remained unclear how diverse RNAs associate with and regulate PRC2. Here, we show that a single-stranded G-rich RNA and an atypical G4 structure called pUG-fold unexpectedly also mediate near-identical PRC2 dimerization resulting in inhibition of PRC2 methyltransferase activity. The conformational flexibility of arginine-rich loops within subunits EZH2 and AEBP2 of PRC2 can accommodate diverse RNA secondary structures, resulting in protein-RNA and protein-protein interfaces similar to those observed previously with G4 RNA. Furthermore, we address a recent report that failed to detect PRC2-associated RNAs in living cells by demonstrating the insensitivity of PRC2-RNA interaction to photochemical crosslinking. Our results support the significance of RNA-mediated PRC2 regulation by showing that this interaction is not limited to a single RNA secondary structure, consistent with the broad PRC2 transcriptome containing many G-tract RNAs incapable of folding into G4 structures.

INTRODUCTION

In the last decade, non-canonical RNA binding proteins that do not contain conventional RNA-recognition or RNA-binding motifs have been of increasing interest. Examples include histone modifiers [1,2], chromatin architecture remodelers [3-5], DNA methylases [6,7], transcription factors [8-10] and metabolic proteins [11,12], many of which participate in tuning differential expression of genes. The binding of RNA has been reported to have various functions, including promoting complex recruitment and enhancing target recognition specificity as a positive regulator, and on the other hand, inhibiting enzymatic activity and limiting target accessibility as a negative regulator, emphasizing the under-characterized but critical role of RNA in epigenetic regulation.

The histone methyltransferase Polycomb Repressive Complex 2 (PRC2) is a prevailing model system for studying the mechanism and significance of RNA binding to epigenetic modifiers [13-15]. PRC2 trimethylates lysine 27 of histone H3 (H3K27me3), which is a repressive mark for gene expression and essential for normal development and cell differentiation [16,17]. Studies have

shown that G-quadruplex (G4) RNAs bind PRC2 to inhibit its activity in cells [18-21], and our recent cryo-EM structure of a G4 RNA-bound PRC2 complex revealed the molecular mechanism of such inhibition [22]. Instead of steric blocking of PRC2's chromatin binding, the G4 RNA bridges two PRC2 protomers to form a dimer that specifically buries PRC2 amino acids required for docking to histone H3 tail and binding nucleosomal DNA. However, the PRC2 interactome has been reported to contain thousands of pre-mRNAs and lncRNAs, and it includes RNAs with fewer than the four G-tracts required to fold into a G4 structure [20,23-30]. These non-G4 RNAs differ from canonical G4 structures in shape, charge distribution, and availability of H-bond donors/acceptors, raising the questions of how PRC2 recognizes various RNA structures and what are the functional consequences of PRC2 associating with these different RNAs.

Here, we use cryo-EM and biochemical methods to investigate PRC2 inhibition by non-G4 RNAs. Surprisingly, all tested RNAs that bound to PRC2 induced PRC2 dimerization. Flexible loops of PRC2 accommodate different RNA structures, showing how RNA beyond G4 can inhibit PRC2 via a molecular mechanism similar to that of G4 RNA. These observations encouraged us to reinvestigate recent work which utilized 254 nm UV crosslinking as the principal methodology and concluded that PRC2-RNA binding did not occur in living cells [31]. We find that this failure to detect PRC2-associated RNA must be considered in light of the very low crosslinking sensitivity of the PRC2-RNA interaction. Overall, our study expands RNA-mediated PRC2 regulation to multiple RNA elements, enhancing the understanding of how diverse RNAs can regulate PRC2 activity.

RESULTS

PRC2 interacts with various RNA secondary structures

The six-subunit PRC2 complex was prepared with full-length EZH2, SUZ12, RBAP48, EED, short-isoform AEBP2, and truncated JARID2$_{119–450}$. Four 50-nucleotide RNA oligos were synthesized (Fig 1A). TERRA contains four repeats of the human telomeric sequence and can form a single G4 structure, mimicking native RNA transcripts generated from the telomeres essential to recruit PRC2 for depositing H3K27me3 marks at telomeric heterochromatin [32]. TERRA$_{mut}$ is a single-stranded G-rich RNA that has the same base composition as TERRA, but the sequence is mutated to eliminate consecutive guanines. The pUG-fold RNA has 20 repeats of GU, sufficient to form an atypical RNA quadruplex, which differs from the canonical G4 by having three G quartets (stacking G tetrads are separated by looped-out U nucleotides) and one additional U quartet [33]. Finally, poly(A) does not bind to the five-subunit PRC2 [29] and is expected to serve as a negative control in our characterization of the six-subunit complex. Native gel electrophoresis confirmed the formation of RNA secondary structures in TERRA and pUG-fold RNAs (Fig 1B), although pUG-fold was only partially folded under these conditions.

Although PRC2-RNA binding has been studied previously [29,34-37], we sought to extend these analyses to the six-subunit complex containing accessory proteins AEBP2 and JARID2 because these accessory proteins have previously been implicated in RNA binding [18,38]. We also sought to provide side-by-side comparisons of the RNAs that we would subject to structural analysis. To this end, we used electrophoretic mobility shift assays (EMSA) with PRC2 and various RNAs incubated in 100 mM KCl to match nuclear ionic conditions, stabilizing G4 structures. PRC2

bound TERRA with the highest affinity, approximately 3-fold stronger than the single-stranded $TERRA_{mut}$ (Fig. 1C). The difference in affinity was in the same direction but only half as large as that reported for five-subunit PRC2 (K_d(TERRA)=80±10 nM vs. K_d($TERRA_{mut}$)=490±20 nM [29]). pUG-fold had an intermediate affinity between TERRA and $TERRA_{mut}$, plausibly due to its incomplete folding. Poly(A), in contrast, did not interact with six-subunit PRC2. When binding was instead performed in 100 mM LiCl to preclude G4 formation, the three G-rich RNAs bound PRC2 with similar affinities (K_d=50-70 nM) and poly(A) remained unbound (Fig. S1). Thus, although the six-subunit complex retained the preference of PRC2 binding the folded G4 RNA, the more modest effect of RNA mutations (TERRA/$TERRA_{mut}$) and K^+/Li^+ substitution indicated that the six-subunit complex bound RNA structures more broadly than the five-subunit complex. More generally, the biochemical results remained consistent with in vivo results showing a broad PRC2 transcriptome containing many lncRNAs and pre-mRNAs [20,24,26,27,39,40].

RNA beyond G4 can mediate PRC2 dimerization

We recently adapted the streptavidin-affinity EM grid method [41] to allow specific selection and enrichment of ribonucleoprotein (RNP) complexes [22]. Here, we synthesized 5'-biotinylated RNAs and applied negative-staining EM to determine the architectures of PRC2 bound to different RNA secondary structures (Fig 2A). Notably, 2D-class averages of PRC2-TERRA, PRC2-$TERRA_{mut}$ and PRC2-pUG-fold RNPs exhibited PRC2 dimerization with similar protomer arrangement as shown in the cryo-EM structure of the $(GGGAA)_4$ G4 RNA-mediated PRC2 dimer [22]. The finding that $TERRA_{mut}$ could mediate PRC2 dimerization was particularly surprising, given that it bears no resemblance to a folded G4 RNA with respect to shape, hydrogen bond donor/acceptor potential or electrostatic charge distribution. In contrast, poly(A) did not substantially capture any particles on the affinity grid (Fig S2), validating the selection of RNP complexes during grid preparations. We quantified two negative-staining EM replicates of each PRC2-RNA complex and found that dimerized PRC2 consistently comprised 70% to 90% of all recognized particles (Fig 2B).

To compare the PRC2 dimers induced by distinct RNA structures, we solved a 3.3 Å cryo-EM structure of the single-stranded $TERRA_{mut}$-bound PRC2 (Fig 2C, Fig S3 and S4, Table S1). In this structure, the PRC2 dimer had the identical architecture as the G4 RNA-mediated complex, including the protein-protein interface assembled by the CXC domain of the catalytic subunit EZH2. This dimer interface is key to explaining RNA inhibition of PRC2 activity because it buries amino acids that are required for histone H3 tail and nucleosome binding in the active PRC2 monomer.

We can confidently identify one $TERRA_{mut}$ RNA density, suggesting a single $TERRA_{mut}$ is sufficient to induce PRC2 dimerization. Because PRC2 utilizes flexible loops to engage RNA, allowing multiple RNA orientations and conformations, we could not obtain high-resolution details to de novo model $TERRA_{mut}$. The location of $TERRA_{mut}$ RNA partially overlaps with the location of G4 RNA from our previous cryo-EM reconstruction (Fig S5). This can be explained if both PRC2 protomers contribute to RNA binding like a pincer. Therefore, the RNA is suspended in the middle of the two PRC2 protomers; there is, in fact, low-resolution density detected both in the PRC2-$TERRA_{mut}$ RNP and the PRC2-G4 RNP. Notably, $TERRA_{mut}$ density is attached to the bottom lobe of one PRC2 protomer in a region of RBAP48, which was unstructured in the

G4 RNA-bound map (Fig S5). This difference may indicate that the single-stranded $TERRA_{mut}$, expected to be more extended than a G4, interacts with additional protein surfaces. Overall, the use of flexible loops to bind RNA, the formation of a dimer with RNA suspended between the protomers, and the additional protein surfaces available for extended RNA elements appear to provide PRC2 the potential to accommodate disparate RNA structures.

AEBP2 is implicated in contributing to non-G4 RNA binding

Because the details of RNA-protein interaction were not resolved in the cryo-EM structure, we used AlphaFold3 [42] to generate models of $TERRA_{mut}$ RNA bound to a single PRC2. We could not model the PRC2 dimer because two copies of PRC2 exceed the input limit of 5000 residues in the AlphaFold Server. In parallel to AlphaFold, we performed multibody refinement of our cryo-EM consensus map to focus on the single PRC2 protomer that interacted with $TERRA_{mut}$, which could be directly compared to the AlphaFold models. The overall PRC2 subunit organization was consistent among all predictions and agreed well with published PRC2 structures [43-49], while $TERRA_{mut}$ RNA had different conformations and orientations with respect to PRC2 in the different predicted models (Fig S6, A-D). AlphaFold3 predictions had high confidence for PRC2 subunits (chain iPTMs=0.4-0.6) and low confidence for $TERRA_{mut}$ (chain iPTM=0.1). In spite of this low confidence, it was gratifying to see that the predicted $TERRA_{mut}$ always overlapped with the density we designated as the RNA in our cryo-EM reconstruction. To better present this feature, we generated a surface map including only regions overlapping between all top AlphaFold models (Fig 2D and Fig S6E); this eliminated flexible regions of the RNA, similar to the principle used in cryo-EM reconstruction that averages several hundred thousand particles. This surface map had identical architecture to the actual cryo-EM map, particularly with only part of $TERRA_{mut}$ being visualized, explaining how the intrinsic flexibility of PRC2-RNA binding affects our EM map.

AlphaFold3 also predicted that PRC2 accessory protein AEBP2 utilizes zinc-finger motifs and an arginine-rich segment (KRRKLKNKRRR) to bind $TERRA_{mut}$ RNA. The second and third C2H2-type zinc-finger motifs within AEBP2 are in the periphery of the RNA, engaging RNA via electrostatic interactions with the phosphate backbone and via hydrogen bonds with both backbone and bases (Fig S7). The residues responsible for this interaction differ between models, indicating that unlike typical zinc-finger motifs that recognize specific DNA sequences, AEBP2 zinc-finger motifs have less strict RNA sequence specificity. In addition, the arginine-rich segment of AEBP2 contains 9 positive-charged amino acids, showing a strong electrostatic potential to bind many RNAs.

To test the prediction that AEBP2 contributed to binding single-stranded G-tract RNAs, we prepared the PRC2 four-subunit holoenzyme (missing accessory proteins AEBP2 and JARID2) and found that it had reduced binding affinity for $TERRA_{mut}$ RNA but not TERRA or pUG-fold RNAs (Fig S8). For four-subunit PRC2, the $K_d(TERRA_{mut})/K_d(TERRA)$ ratio was 12, substantially larger than the ratio of 3.7 obtained for the six-subunit complex, consistent with AEBP2 making additional interactions with the $TERRA_{mut}$ RNA. Thus, accessory proteins enable PRC2 to accommodate diverse RNAs, including single-stranded G-rich RNA.

RNAs that induce dimerization inhibit PRC2 activity

Most biochemical characterizations of RNA-mediated PRC2 inhibition have focused on short G4-forming sequences [18,21,22,37,50] and long RNAs that likely fold into complex 3D architectures containing multiple structural elements (e.g., HOTAIR and Xist lncRNAs) [18,20,35,51]. The effect of simple G-tract sequences other than canonical G4 on PRC2 activity has not been measured.

Therefore, we performed methyltransferase assays of PRC2 with our RNAs of defined structures (Figure 3). We found a progressive reduction of H3K27 methylation when we included TERRA, $TERRA_{mut,}$ and pUG-fold RNAs in trans, but no change with the poly(A) negative control. IC_{50} of TERRA, $TERRA_{mut}$, and pUG-fold RNA were all around 500 nM, and complete inhibition was achieved at high RNA concentrations. (Because the activity is assayed at PRC2 concentrations above the K_d for PRC2-RNA binding, IC_{50} is higher than the K_d.) Considering that all three G-rich RNAs we tested mediate the same mode of PRC2 dimerization, we conclude that it is the RNA-induced PRC2 dimerization that inhibits PRC2 activity, independent of the secondary structure of the RNA that is bound.

PRC2-RNA interactions are insensitive to UV crosslinking

Studies of PRC2 in living cells have reported the importance of G-rich RNA in PRC2 inhibition, e.g., chromatin-associated G-tract RNA removes PRC2 from specific genes during gene activation [20,39]; G-tract RNA tethering can activate a PRC2-silienced gene and induce cell senescence [19]; and deletion of Xist G4 elements leads to hyper-enrichment of H3K27me3 [21]. These reports are consistent with our structural and biochemical characterizations that in turn illuminate the molecular mechanism of RNA inhibition. However, a recent publication failed to capture RNAs bound to PRC2 in living cells [31], thereby challenging these widespread reports of PRC2-RNA interaction. Those authors modified the conventional CLIP assay to a method called CLAP (covalent linkage and affinity purification), which allows denaturing washes prior to the identification of protein-associated RNA. Like CLIP, CLAP is completely dependent on 254 nm UV crosslinking. UV crosslinking is known to be biased towards uracil [52-54] and towards certain amino acids [55-57], and highly sensitive to the precise distance and orientation of RNA base relative to protein amino acid [55,56,58,59]. For example, RNA recognition motifs (RRMs), which rely on the stacking interaction between aromatic amino acids and RNA bases, are UV-crosslinked with unusually high efficiency, dominating CLIP-seq databases [57]. Therefore, we suspected that the efficiency of UV crosslinking might not be sufficient to covalently link PRC2 to RNAs bound to it in cells, given that PRC2 uses flexible arginine-rich loops to interact with G-tract RNA.

To test this hypothesis, we performed in vitro UV crosslinking assays of PRC2 with different RNAs (Fig 4). We also included the positive control used in *Guo et al.*, namely PTBP1 (Polypyrimidine Tract-Binding Protein 1), which harbors four canonical RRMs and interacts with a defined U-rich RNA consensus UCUUUCU [60]. We incubated 600 nM PTBP1 or PRC2 each with their cognate RNAs at concentrations 10 times greater than the K_d values to ensure saturated binding in all reactions (Fig S9). The PTBP1-$(UCUUUCU)_6$ interaction was efficiently crosslinked at energies from 0.028 J/cm^2 to 0.5 J/cm^2 (Fig 4B), including 0.25 J/cm^2 which is frequently applied to intact cells and was used in *Guo et al.* In the PRC2 reactions, we selected the RNA termed 2G4 used in the initial cryo-EM determination of a PRC2-RNA complex; this RNA can assemble into two independent G4 structures and binds PRC2 ($K_{d\ 2G4}$=32±4 nM [22]), but does not contain any uracil in the G4 sequence (Fig 4A). We also examined TERRA and

$TERRA_{mut}$ RNAs, which, although not uracil-rich like the PTBP1-consensus RNA, contain a few U bases. We found that PRC2 did not effectively crosslink to any of these three RNAs up to 0.5 J/cm^2 energy, substantially distinct from PTBP1 (Fig 4B). Although 2G4 has strong affinity for binding to PRC2, it had the least crosslinked proportion among the three RNAs we tested, presumably because the absence of uracil limited UV crosslinking. The intrinsic inefficiency of PRC2 UV-crosslinking to its preferred RNA partners may explain the failure to capture PRC2-RNA complexes by the CLAP technique.

An additional consideration is that, unlike PTBP1, which binds only RNA, PRC2 binds RNA and DNA. Therefore, competition from nucleosomal DNA might limit the proportion of RNA-bound PRC2 in cell nuclei. To evaluate this possibility, we performed EMSA to test six-subunit PRC2 and four-subunit core complex binding to double-stranded DNA consisting of the $TERRA_{mut}$ sequence bound to its complement (Fig S10). PRC2 bound this dsDNA 10-fold more weakly than RNA. We also tested ssDNA with either the TERRA sequence (G4 DNA) or $TERRA_{mut}$ sequence (non-G4 DNA), and no binding was detected up to 1 uM concentration. Furthermore, we and others previously found that nucleosomes, the true substrate of PRC2, bind weakly and cannot compete with RNA for PRC2 binding [20,22,50]. The intrinsically stronger binding of PRC2 to RNA than to DNA and nucleosomes supports the conclusion that PRC2 is likely to bind RNA in cell nuclei.

DISCUSSION

Previous studies of PRC2-associated RNAs validate the biological importance of RNA binding in the precise control of PRC2 activity [18,19,21]. Inhibition of PRC2 activity by nascent RNA is thought to help maintain epigenetic gene silencing, ensuring that PRC2 adds its repressive histone mark only at those genes already silenced at the transcriptional level. The sequence and structural diversity of these nascent RNAs raises the question of how PRC2 can recognize RNA targets without a strict sequence consensus.

Here, we show that two different G-rich RNA secondary structures, although binding with lower affinity compared to G4, can mediate PRC2 dimerization and inhibit PRC2 catalytic activity through a mechanism similar to the G4 RNA. Both of these RNAs contain 50% guanine but no consecutive G nucleotides; $TERRA_{mut}$ is an unstructured single strand, while the p(UG)fold forms a non-canonical G4 structure. Our structural analysis indicates that the flexible positively charged loops of PRC2 suspend each of these RNA between two PRC2 protomers with the ability to accommodate different RNA secondary structures.

Despite G4 RNA being predominantly studied for PRC2-RNA interaction, many independent research groups have investigated other RNA sequences, including HOTAIR RNA [61-63], Repeat A motif of Xist [35,64], RNA transcribed from B2 SINE retrotransposon [65,66], and artificial sequences without continuous G-tracts [29,37]. Deep sequencing analyses of RNA motifs bound by PRC2 identified shorter G-tract motifs incapable of folding into G4 in addition to the G4-forming tracts [29,30]. Our results support this conclusion that G4 is not necessary for RNA to bind and regulate PRC2.

Our previous structural characterization of the G4 RNA-bound PRC2 presented the first use of streptavidin-affinity EM grid method for an RNP complex [22], a technical advance that selected

the desired complex and enhanced particle quality by holding particles away from the denaturing water-air interface [41,67]. In this work, we tested this technique with more challenging RNPs composed of less tightly bound RNAs. The successful negative staining and cryo-EM results support the potential of this method to obtain structural information of less preferred minor populations and even transiently interacting complexes. Another new analysis utilized here was integrating AlphaFold3 predictions to illustrate the flexibility of RNA conformations and orientations in our complex. AlphaFold3 has provided the ability to predict protein-nucleic acid interactions for multi-protein complexes. The high similarity between the AlphaFold3 models and our experimental cryo-EM density highlights the accuracy of its prediction. Furthermore, it provided clues for testing the role of PRC2 accessory protein AEBP2 in accommodating single-stranded RNA, which could not be interpreted directly from our cryo-EM map. These new methods are likely to facilitate many future studies of other non-canonical protein-RNA interactions.

After the success of the CLIP assay, UV crosslinking has been considered the gold standard to covalently fix protein-RNA interactions before cell lysis and identify protein-associated RNAs present in living cells [68]. Despite these prevalent applications of protein-RNA photochemical crosslinking, the underlying biophysical and chemical principles are poorly understood. It is unambiguous, however, that UV crosslinking is biased towards certain types of protein-RNA interactions. Stacking between the aromatic side chain of defined amino acids and uracil is advantageous for photocrosslinking [55]. *Knorlein et al.* reported that up to 78% of UV-crosslinked sites in RNP complexes with available structural information were mapped to interactions by base stacking with aromatic residues [57]. In addition to amino acids, RNA nucleotide sequence and conformation have been implicated to have different sensitivity to photochemical crosslinking [52-56,58,59,69]. Our in vitro crosslinking assays support these conclusions in which RRM-harboring protein PTBP1 could be crosslinked to U-rich RNA more than an order-of-magnitude better than PRC2, which instead utilizes arginine-rich flexible loops to bind G-tract RNA. Considering the extremely variable efficiency of UV crosslinking, relying on UV crosslinking before denaturing washes to select covalently crosslinked RNA in the CLAP assay will work for some protein-RNA complexes and not for others. Based on these results, we urge caution in making conclusions from a negative CLAP result, as negating the intrinsic RNA-binding potential of many non-canonical RNA-binding proteins may be unwarranted.

LIMITATIONS OF THE STUDY

Although we used specialized cryo-EM preparation and processing methods, $TERRA_{mut}$ RNA and peripheral protein regions in our density map did not reach high resolution. We cannot unambiguously model $TERRA_{mut}$ and demonstrate the exact amino acid residues within PRC2 flexible loops responsible for RNA binding. In addition, AlphaFold3 could not predict $TERRA_{mut}$ RNA interactions with PRC2 subunits with high confidence (chain iPTM and chain-pair iPTM < 0.2). Although the predicted AEBP2-RNA interactions are consistent between models, the details of this interaction differ. Our data cannot provide an atomic model to illustrate how zinc-finger domains of AEBP2 bind RNA. Finally, our results do not address the possibility that in some cases of sparse transcription, RNA might be able to recruit PRC2 to chromatin (reviewed in [13,70]), an activity that is biophysically possible [71] but difficult to test in cells.

DECLARATION OF INTERESTS

T.R.C is a scientific advisor for Storm Therapeutics, Eikon Therapeutics, SomaLogic and lincSwitch Therapeutics. The other authors declare no interests.

ACKNOWLEDGEMENTS

We thank E. Hartwick and S. Laursen (University of Colorado Boulder Biochemistry Krios Electron Microscopy Facility RRID: SCR_019057) for cryo-EM data collection and storage infrastructure maintenance. We thank S. Zimmermann and G. Morgan (University of Colorado Boulder Electron Microscopy Service) for negative staining data collection. We thank A. Erbse (University of Colorado Boulder Shared Instruments Pool RRID SCR_018986) for providing research instrumentation, in particular the Avanti JXN 26 centrifuge (funded by NIH Grant R24OD033699-01). We thank T. Nahreini (University of Colorado Boulder Cell Culture Facility RRID:SCR_018988) for use of the cell culture facility.

FUNDING

J.S. is supported by Howard Hughes Medical Institute–Jane Coffin Childs postdoctoral fellowship. L.Y. and V.K are supported by R00GM132544, R35GM155426, and CU Boulder start-up funds. T.R.C. is an investigator of the Howard Hughes Medical Institute.

DATA AND MATERIALS AVAILABILITY

Cryo-EM density maps and fitted models have been deposited in the Electron Microscopy Data Bank (EMD-46751, consensus map; EMD-46722, Body1 from multibody refinement; and EMD-46726, Body2 from multibody refinement) and the Protein Data Bank (PDB: 9DCH). Requests for reagents, plasmids, cell lines, and zebrafish strains used in this study should be directed to the corresponding authors.

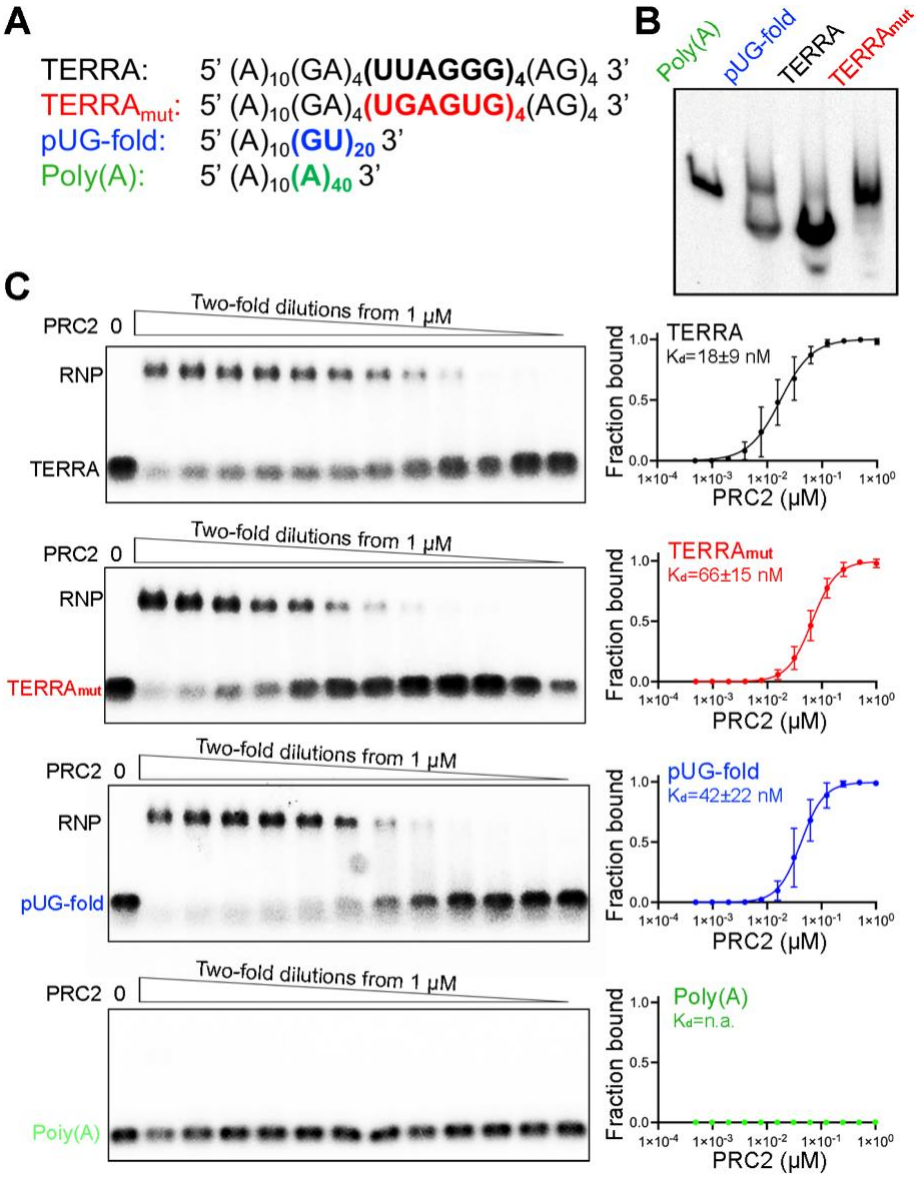

Figure 1. PRC2 binds RNAs of various secondary structures. (A) The four RNA oligonucleotides used in this study. Colored sequences highlight the functional elements within RNA oligos. $(A)_{10}$ linker sequences provide flexibility for binding to streptavidin EM grids. (B) Native gel electrophoresis of RNA. RNAs were folded in K^+ buffer and then analyzed using a native polyacrylamide gel run in K^+-containing buffer. (C) Left: representative EMSA gels of PRC2 and the four RNAs. Right: quantification of three EMSA replicates. Error bars are mean ± standard deviation.

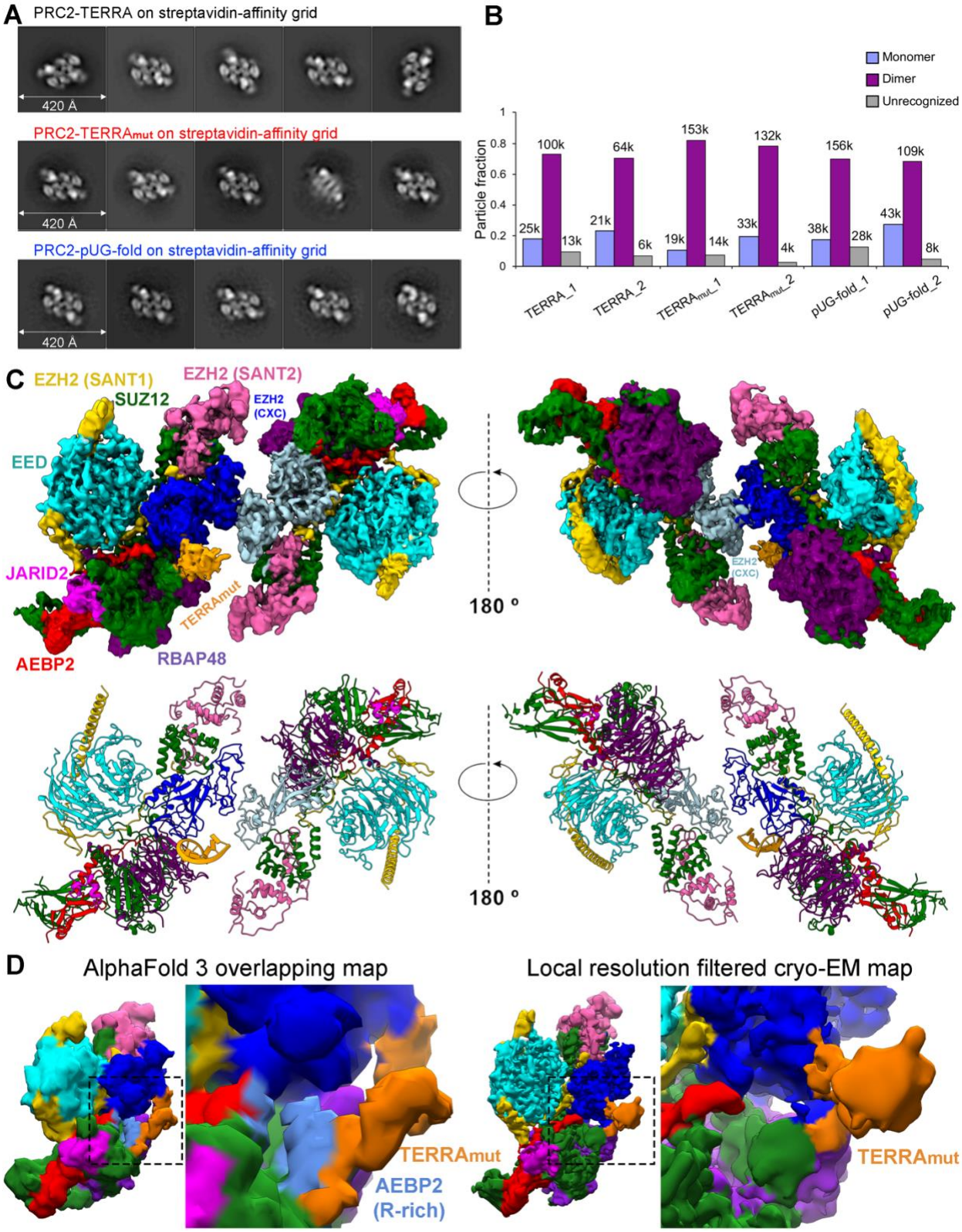
A
PRC2-TERRA on streptavidin-affinity grid
420 Å
PRC2-TERRAmut on streptavidin-affinity grid
420 Å
PRC2-pUG-fold on streptavidin-affinity grid
420 Å
B
Monomer
Dimer
Unrecognized
Particle fraction
1
0.8
0.6
0.4
0.2
0
25k
100k
13k
21k
64k
6k
19k
153k
14k
33k
132k
4k
38k
156k
28k
43k
109k
8k
TERRA_1
TERRA_2
TERRAmut_1
TERRAmut_2
pUG-fold_1
pUG-fold_2
C
EZH2 (SANT1)
EZH2 (SANT2)
SUZ12
EZH2 (CXC)
EED
JARID2
TERRAmut
AEBP2
RBAP48
180 °
EZH2 (CXC)
180 °
D
AlphaFold 3 overlapping map
Local resolution filtered cryo-EM map
TERRAmut
AEBP2 (R-rich)
TERRAmut

Figure 2. RNAs beyond G4s induce PRC2 dimerization. (A) Negative-staining EM provided 2D-class averages of PRC2-TERRA, PRC2-$TERRA_{mut}$, and PRC2-pUG-fold complexes, which all exhibit dimerization of PRC2. The 2D-class averages are shown in order of prevalence from left to right. (B) Quantification of two negative-staining EM replicates (two independent EM grids, each grid utilizing PRC2 from a separate preparation). (C) Top: Cryo-EM density map of $TERRA_{mut}$ RNA-associated PRC2 dimer. EZH2 (CXC-SET) of protomer 1 in blue, EZH2 (CXC-SET) of protomer 2 in light blue, and $TERRA_{mut}$ RNA in orange. Bottom: The corresponding atomic model. (D) Left: Density map generated by keeping only the overlapped regions of the top four AlphaFold3 models (Fig S6) (see Methods). Right: Local resolution filtered cryo-EM density from multibody refinement of $TERRA_{mut}$ RNA-associated PRC2. Dashed boxes are zoomed in. The remaining density of $TERRA_{mut}$ after averaging AlphaFold models has similar size and position comparing to the observed cryo-EM density.

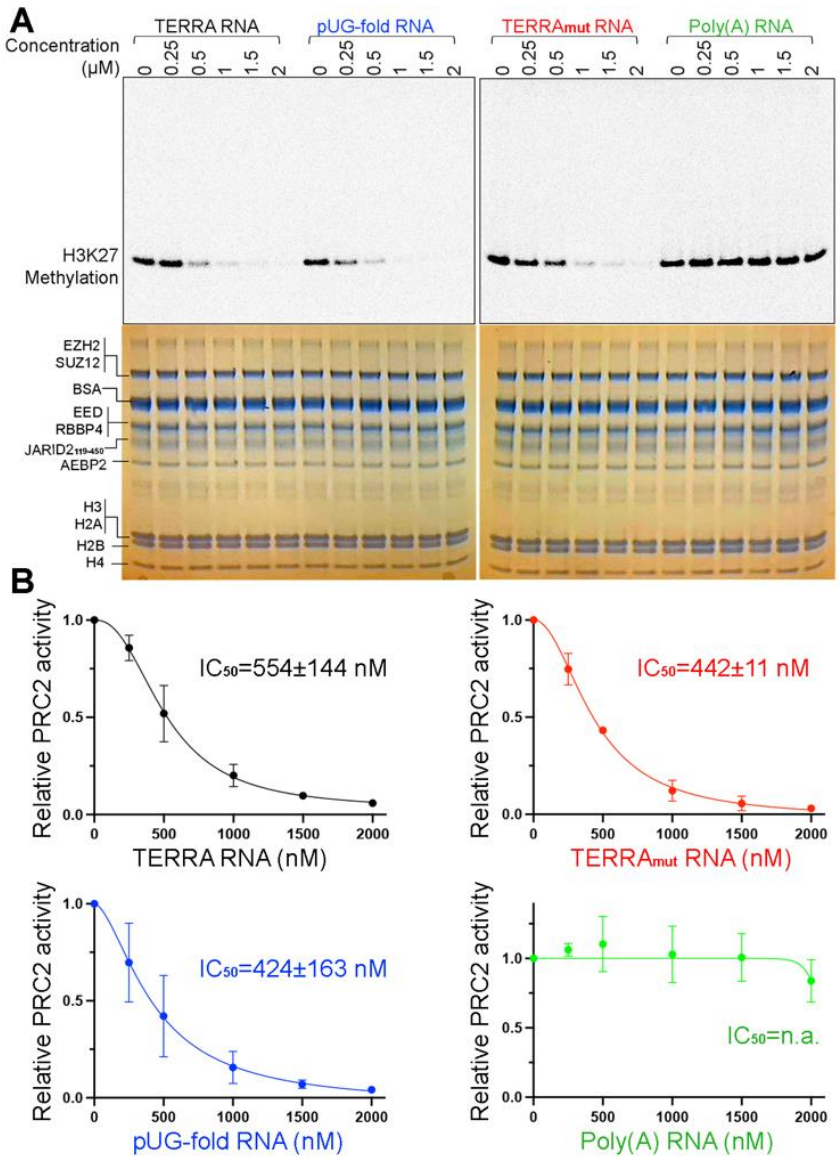

Figure 3. RNAs beyond G4s inhibit histone methyltransferase activity of PRC2 6-subunit complex. (A) Representative histone methyltransferase activity assays with ^{14}C-labeled S-adenosylmethionine analyzed by SDS-PAGE, with gels imaged for ^{14}C (top) or stained with Coomassie blue to confirm equal loading of PRC2 and nucleosomes (bottom). (B) Quantification of three replicates. Error bars are mean ± standard deviation. IC_{50} is the concentration of RNA that inhibits 50% of PRC2 activity relative to no RNA.

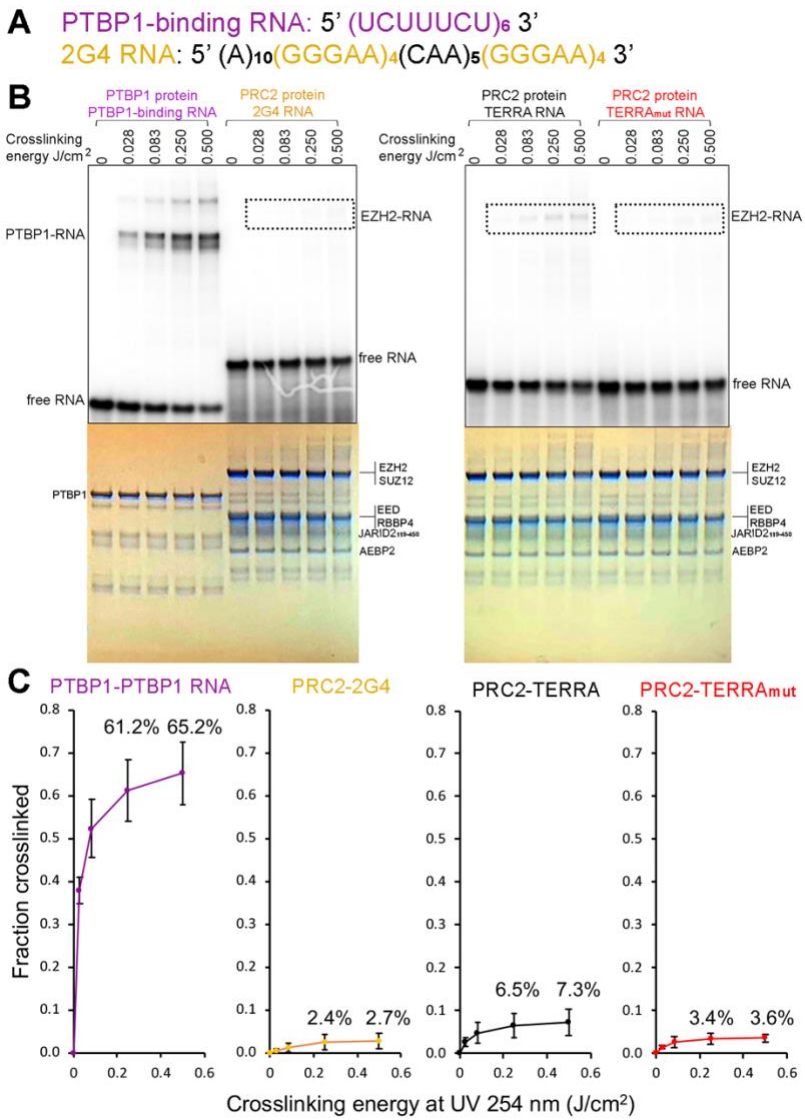

Figure 4. UV crosslinking is insufficient to capture PRC2-RNA association. (A) Sequences of RNA oligos used in this assay. (B) Representative UV crosslinking assays. In all reactions, proteins were 0.6 μM (at least 10-times K_d) to ensure saturated RNA-binding. Gels were imaged to reveal crosslinking of radiolabeled RNA (top) or stained with Coomassie blue to confirm equal loading of proteins (bottom). Dashed boxes are positions expected for crosslinked EZH2-RNA complexes. (C) Quantification of three UV crosslinking replicates. Error bars are mean ± standard deviation.

REFERENCES

1. Guttman, M., Donaghey, J., Carey, B.W., Garber, M., Grenier, J.K., Munson, G., Young, G., Lucas, A.B., Ach, R., Bruhn, L., et al. (2011). lincRNAs act in the circuitry controlling pluripotency and differentiation. Nature *477*, 295-300. 10.1038/nature10398.
2. Long, Y., Wang, X., Youmans, D.T., and Cech, T.R. (2017). How do lncRNAs regulate transcription? Sci Adv *3*, eaao2110. 10.1126/sciadv.aao2110.
3. Hansen, A.S., Hsieh, T.S., Cattoglio, C., Pustova, I., Saldana-Meyer, R., Reinberg, D., Darzacq, X., and Tjian, R. (2019). Distinct Classes of Chromatin Loops Revealed by Deletion of an RNA-Binding Region in CTCF. Mol Cell *76*, 395-411 e313. 10.1016/j.molcel.2019.07.039.
4. Jegu, T., Blum, R., Cochrane, J.C., Yang, L., Wang, C.Y., Gilles, M.E., Colognori, D., Szanto, A., Marr, S.K., Kingston, R.E., and Lee, J.T. (2019). Xist RNA antagonizes the SWI/SNF chromatin remodeler BRG1 on the inactive X chromosome. Nat Struct Mol Biol *26*, 96-109. 10.1038/s41594-018-0176-8.
5. Seczynska, M., and Lehner, P.J. (2023). The sound of silence: mechanisms and implications of HUSH complex function. Trends Genet *39*, 251-267. 10.1016/j.tig.2022.12.005.
6. Di Ruscio, A., Ebralidze, A.K., Benoukraf, T., Amabile, G., Goff, L.A., Terragni, J., Figueroa, M.E., De Figueiredo Pontes, L.L., Alberich-Jorda, M., Zhang, P., et al. (2013). DNMT1-interacting RNAs block gene-specific DNA methylation. Nature *503*, 371-376. 10.1038/nature12598.
7. Jansson-Fritzberg, L.I., Sousa, C.I., Smallegan, M.J., Song, J.J., Gooding, A.R., Kasinath, V., Rinn, J.L., and Cech, T.R. (2022). DNMT1 inhibition by pUG-fold quadruplex RNA. RNA. 10.1261/rna.079479.122.
8. Holmes, Z.E., Hamilton, D.J., Hwang, T., Parsonnet, N.V., Rinn, J.L., Wuttke, D.S., and Batey, R.T. (2020). The Sox2 transcription factor binds RNA. Nat Commun *11*, 1805. 10.1038/s41467-020-15571-8.
9. Oksuz, O., Henninger, J.E., Warneford-Thomson, R., Zheng, M.M., Erb, H., Overholt, K.J., Hawken, S.W., Banani, S.F., Lauman, R., Vancura, A., et al. (2022). Transcription factors interact with RNA to regulate genes. bioRxiv, 2022.2009.2027.509776. 10.1101/2022.09.27.509776.
10. Steiner, H.R., Lammer, N.C., Batey, R.T., and Wuttke, D.S. (2022). An Extended DNA Binding Domain of the Estrogen Receptor Alpha Directly Interacts with RNAs in Vitro. Biochemistry *61*, 2490-2494. 10.1021/acs.biochem.2c00536.
11. Nagy, E., and Rigby, W.F. (1995). Glyceraldehyde-3-phosphate dehydrogenase selectively binds AU-rich RNA in the NAD(+)-binding region (Rossmann fold). J Biol Chem *270*, 2755-2763. 10.1074/jbc.270.6.2755.
12. Anastasakis, D.G., Apostolidi, M., Garman, K.A., Polash, A.H., Umar, M.I., Meng, Q., Scutenaire, J., Jarvis, J.E., Wang, X., Haase, A.D., et al. (2024). Nuclear PKM2 binds pre-mRNA at folded G-quadruplexes and reveals their gene regulatory role. Mol Cell. 10.1016/j.molcel.2024.07.025.
13. Davidovich, C., and Cech, T.R. (2015). The recruitment of chromatin modifiers by long noncoding RNAs: lessons from PRC2. RNA *21*, 2007-2022. 10.1261/rna.053918.115.
14. Yan, J., Dutta, B., Hee, Y.T., and Chng, W.J. (2019). Towards understanding of PRC2 binding to RNA. RNA Biol *16*, 176-184. 10.1080/15476286.2019.1565283.
15. Iwasaki, Y.W., Koseki, H., and Ito, S. (2023). In preprints: revisiting RNA in PRC2. Development *150*. 10.1242/dev.202440.
16. Margueron, R., and Reinberg, D. (2011). The Polycomb complex PRC2 and its mark in life. Nature *469*, 343-349. 10.1038/nature09784.
17. Blackledge, N.P., and Klose, R.J. (2021). The molecular principles of gene regulation by Polycomb repressive complexes. Nat Rev Mol Cell Biol *22*, 815-833. 10.1038/s41580-021-00398-y.
18. Kaneko, S., Son, J., Bonasio, R., Shen, S.S., and Reinberg, D. (2014). Nascent RNA interaction keeps PRC2 activity poised and in check. Genes Dev *28*, 1983-1988. 10.1101/gad.247940.114.
19. Beltran, M., Tavares, M., Justin, N., Khandelwal, G., Ambrose, J., Foster, B.M., Worlock, K.B., Tvardovskiy, A., Kunzelmann, S., Herrero, J., et al. (2019). G-tract RNA removes Polycomb repressive complex 2 from genes. Nat Struct Mol Biol *26*, 899-909. 10.1038/s41594-019-0293-z.

20. Beltran, M., Yates, C.M., Skalska, L., Dawson, M., Reis, F.P., Viiri, K., Fisher, C.L., Sibley, C.R., Foster, B.M., Bartke, T., et al. (2016). The interaction of PRC2 with RNA or chromatin is mutually antagonistic. Genome Res *26*, 896-907. 10.1101/gr.197632.115.
21. Lee, Y.W., Weissbein, U., Blum, R., and Lee, J.T. (2024). G-quadruplex folding in Xist RNA antagonizes PRC2 activity for stepwise regulation of X chromosome inactivation. Mol Cell *84*, 1870-1885 e1879. 10.1016/j.molcel.2024.04.015.
22. Song, J., Gooding, A.R., Hemphill, W.O., Love, B.D., Robertson, A., Yao, L., Zon, L.I., North, T.E., Kasinath, V., and Cech, T.R. (2023). Structural basis for inactivation of PRC2 by G-quadruplex RNA. Science *381*, 1331-1337. 10.1126/science.adh0059.
23. Zhao, J., Sun, B.K., Erwin, J.A., Song, J.J., and Lee, J.T. (2008). Polycomb proteins targeted by a short repeat RNA to the mouse X chromosome. Science *322*, 750-756. 10.1126/science.1163045.
24. Khalil, A.M., Guttman, M., Huarte, M., Garber, M., Raj, A., Rivea Morales, D., Thomas, K., Presser, A., Bernstein, B.E., van Oudenaarden, A., et al. (2009). Many human large intergenic noncoding RNAs associate with chromatin-modifying complexes and affect gene expression. Proc Natl Acad Sci U S A *106*, 11667-11672. 10.1073/pnas.0904715106.
25. Kanhere, A., Viiri, K., Araujo, C.C., Rasaiyaah, J., Bouwman, R.D., Whyte, W.A., Pereira, C.F., Brookes, E., Walker, K., Bell, G.W., et al. (2010). Short RNAs are transcribed from repressed polycomb target genes and interact with polycomb repressive complex-2. Mol Cell *38*, 675-688. 10.1016/j.molcel.2010.03.019.
26. Zhao, J., Ohsumi, T.K., Kung, J.T., Ogawa, Y., Grau, D.J., Sarma, K., Song, J.J., Kingston, R.E., Borowsky, M., and Lee, J.T. (2010). Genome-wide identification of polycomb-associated RNAs by RIP-seq. Mol Cell *40*, 939-953. 10.1016/j.molcel.2010.12.011.
27. Davidovich, C., Zheng, L., Goodrich, K.J., and Cech, T.R. (2013). Promiscuous RNA binding by Polycomb repressive complex 2. Nat Struct Mol Biol *20*, 1250-1257. 10.1038/nsmb.2679.
28. Somarowthu, S., Legiewicz, M., Chillon, I., Marcia, M., Liu, F., and Pyle, A.M. (2015). HOTAIR forms an intricate and modular secondary structure. Mol Cell *58*, 353-361. 10.1016/j.molcel.2015.03.006.
29. Wang, X., Goodrich, K.J., Gooding, A.R., Naeem, H., Archer, S., Paucek, R.D., Youmans, D.T., Cech, T.R., and Davidovich, C. (2017). Targeting of Polycomb Repressive Complex 2 to RNA by Short Repeats of Consecutive Guanines. Mol Cell *65*, 1056-1067 e1055. 10.1016/j.molcel.2017.02.003.
30. Rosenberg, M., Blum, R., Kesner, B., Aeby, E., Garant, J.M., Szanto, A., and Lee, J.T. (2021). Motif-driven interactions between RNA and PRC2 are rheostats that regulate transcription elongation. Nat Struct Mol Biol *28*, 103-117. 10.1038/s41594-020-00535-9.
31. Guo, J.K., Blanco, M.R., Walkup, W.G.t., Bonesteele, G., Urbinati, C.R., Banerjee, A.K., Chow, A., Ettlin, O., Strehle, M., Peyda, P., et al. (2024). Denaturing purifications demonstrate that PRC2 and other widely reported chromatin proteins do not appear to bind directly to RNA in vivo. Mol Cell *84*, 1271-1289 e1212. 10.1016/j.molcel.2024.01.026.
32. Montero, J.J., Lopez-Silanes, I., Megias, D., M, F.F., Castells-Garcia, A., and Blasco, M.A. (2018). TERRA recruitment of polycomb to telomeres is essential for histone trymethylation marks at telomeric heterochromatin. Nat Commun *9*, 1548. 10.1038/s41467-018-03916-3.
33. Roschdi, S., Yan, J., Nomura, Y., Escobar, C.A., Petersen, R.J., Bingman, C.A., Tonelli, M., Vivek, R., Montemayor, E.J., Wickens, M., et al. (2022). An atypical RNA quadruplex marks RNAs as vectors for gene silencing. Nat Struct Mol Biol *29*, 1113-1121. 10.1038/s41594-022-00854-z.
34. Kaneko, S., Li, G., Son, J., Xu, C.F., Margueron, R., Neubert, T.A., and Reinberg, D. (2010). Phosphorylation of the PRC2 component Ezh2 is cell cycle-regulated and up-regulates its binding to ncRNA. Genes Dev *24*, 2615-2620. 10.1101/gad.1983810.
35. Cifuentes-Rojas, C., Hernandez, A.J., Sarma, K., and Lee, J.T. (2014). Regulatory interactions between RNA and polycomb repressive complex 2. Mol Cell *55*, 171-185. 10.1016/j.molcel.2014.05.009.
36. Davidovich, C., Wang, X., Cifuentes-Rojas, C., Goodrich, K.J., Gooding, A.R., Lee, J.T., and Cech, T.R. (2015). Toward a consensus on the binding specificity and promiscuity of PRC2 for RNA. Mol Cell *57*, 552-558. 10.1016/j.molcel.2014.12.017.
37. Zhang, Q., McKenzie, N.J., Warneford-Thomson, R., Gail, E.H., Flanigan, S.F., Owen, B.M., Lauman, R., Levina, V., Garcia, B.A., Schittenhelm, R.B., et al. (2019). RNA exploits an exposed

regulatory site to inhibit the enzymatic activity of PRC2. Nat Struct Mol Biol *26*, 237-247. 10.1038/s41594-019-0197-y.
38. Kaneko, S., Bonasio, R., Saldana-Meyer, R., Yoshida, T., Son, J., Nishino, K., Umezawa, A., and Reinberg, D. (2014). Interactions between JARID2 and noncoding RNAs regulate PRC2 recruitment to chromatin. Mol Cell *53*, 290-300. 10.1016/j.molcel.2013.11.012.
39. Kaneko, S., Son, J., Shen, S.S., Reinberg, D., and Bonasio, R. (2013). PRC2 binds active promoters and contacts nascent RNAs in embryonic stem cells. Nat Struct Mol Biol *20*, 1258-1264. 10.1038/nsmb.2700.
40. Hendrickson, G.D., Kelley, D.R., Tenen, D., Bernstein, B., and Rinn, J.L. (2016). Widespread RNA binding by chromatin-associated proteins. Genome Biol *17*, 28. 10.1186/s13059-016-0878-3.
41. Han, B.G., Watson, Z., Kang, H., Pulk, A., Downing, K.H., Cate, J., and Glaeser, R.M. (2016). Long shelf-life streptavidin support-films suitable for electron microscopy of biological macromolecules. J Struct Biol *195*, 238-244. 10.1016/j.jsb.2016.06.009.
42. Abramson, J., Adler, J., Dunger, J., Evans, R., Green, T., Pritzel, A., Ronneberger, O., Willmore, L., Ballard, A.J., Bambrick, J., et al. (2024). Accurate structure prediction of biomolecular interactions with AlphaFold 3. Nature *630*, 493-500. 10.1038/s41586-024-07487-w.
43. Kasinath, V., Faini, M., Poepsel, S., Reif, D., Feng, X.A., Stjepanovic, G., Aebersold, R., and Nogales, E. (2018). Structures of human PRC2 with its cofactors AEBP2 and JARID2. Science *359*, 940-944. 10.1126/science.aar5700.
44. Kasinath, V., Beck, C., Sauer, P., Poepsel, S., Kosmatka, J., Faini, M., Toso, D., Aebersold, R., and Nogales, E. (2021). JARID2 and AEBP2 regulate PRC2 in the presence of H2AK119ub1 and other histone modifications. Science *371*. 10.1126/science.abc3393.
45. Poepsel, S., Kasinath, V., and Nogales, E. (2018). Cryo-EM structures of PRC2 simultaneously engaged with two functionally distinct nucleosomes. Nat Struct Mol Biol *25*, 154-162. 10.1038/s41594-018-0023-y.
46. Grau, D., Zhang, Y., Lee, C.H., Valencia-Sanchez, M., Zhang, J., Wang, M., Holder, M., Svetlov, V., Tan, D., Nudler, E., et al. (2021). Structures of monomeric and dimeric PRC2:EZH1 reveal flexible modules involved in chromatin compaction. Nat Commun *12*, 714. 10.1038/s41467-020-20775-z.
47. Gong, L., Liu, X., Jiao, L., Yang, X., Lemoff, A., and Liu, X. (2022). CK2-mediated phosphorylation of SUZ12 promotes PRC2 function by stabilizing enzyme active site. Nat Commun *13*, 6781. 10.1038/s41467-022-34431-1.
48. Jiao, L., and Liu, X. (2015). Structural basis of histone H3K27 trimethylation by an active polycomb repressive complex 2. Science *350*, aac4383. 10.1126/science.aac4383.
49. Chen, S., Jiao, L., Shubbar, M., Yang, X., and Liu, X. (2018). Unique Structural Platforms of Suz12 Dictate Distinct Classes of PRC2 for Chromatin Binding. Mol Cell *69*, 840-852 e845. 10.1016/j.molcel.2018.01.039.
50. Wang, X., Paucek, R.D., Gooding, A.R., Brown, Z.Z., Ge, E.J., Muir, T.W., and Cech, T.R. (2017). Molecular analysis of PRC2 recruitment to DNA in chromatin and its inhibition by RNA. Nat Struct Mol Biol *24*, 1028-1038. 10.1038/nsmb.3487.
51. Balas, M.M., Hartwick, E.W., Barrington, C., Roberts, J.T., Wu, S.K., Bettcher, R., Griffin, A.M., Kieft, J.S., and Johnson, A.M. (2021). Establishing RNA-RNA interactions remodels lncRNA structure and promotes PRC2 activity. Sci Adv *7*. 10.1126/sciadv.abc9191.
52. Smith, K.C. (1966). Physical and chemical changes induced in nucleic acids by ultraviolet light. Radiat Res, Suppl 6:54-79.
53. Williams, K.R., and Konigsberg, W.H. (1991). [25] Identification of amino acid residues at interface of protein—Nucleic acid complexes by photochemical cross-linking. In Methods in Enzymology, (Academic Press), pp. 516-539. https://doi.org/10.1016/0076-6879(91)08027-F.
54. Hockensmith, J.W., Kubasek, W.L., Vorachek, W.R., and von Hippel, P.H. (1986). Laser cross-linking of nucleic acids to proteins. Methodology and first applications to the phage T4 DNA replication system. J Biol Chem *261*, 3512-3518.
55. Feng, H., Lu, X.J., Maji, S., Liu, L., Ustianenko, D., Rudnick, N.D., and Zhang, C. (2024). Structure-based prediction and characterization of photo-crosslinking in native protein-RNA complexes. Nat Commun *15*, 2279. 10.1038/s41467-024-46429-y.

56. Vieira-Vieira, C.H., and Selbach, M. (2021). Opportunities and Challenges in Global Quantification of RNA-Protein Interaction via UV Cross-Linking. Front Mol Biosci *8*, 669939. 10.3389/fmolb.2021.669939.
57. Knorlein, A., Sarnowski, C.P., de Vries, T., Stoltz, M., Gotze, M., Aebersold, R., Allain, F.H., Leitner, A., and Hall, J. (2022). Nucleotide-amino acid pi-stacking interactions initiate photo cross-linking in RNA-protein complexes. Nat Commun *13*, 2719. 10.1038/s41467-022-30284-w.
58. Bae, J.W., Kwon, S.C., Na, Y., Kim, V.N., and Kim, J.S. (2020). Chemical RNA digestion enables robust RNA-binding site mapping at single amino acid resolution. Nat Struct Mol Biol *27*, 678-682. 10.1038/s41594-020-0436-2.
59. Kramer, K., Sachsenberg, T., Beckmann, B.M., Qamar, S., Boon, K.L., Hentze, M.W., Kohlbacher, O., and Urlaub, H. (2014). Photo-cross-linking and high-resolution mass spectrometry for assignment of RNA-binding sites in RNA-binding proteins. Nat Methods *11*, 1064-1070. 10.1038/nmeth.3092.
60. Ray, D., Kazan, H., Chan, E.T., Pena Castillo, L., Chaudhry, S., Talukder, S., Blencowe, B.J., Morris, Q., and Hughes, T.R. (2009). Rapid and systematic analysis of the RNA recognition specificities of RNA-binding proteins. Nat Biotechnol *27*, 667-670. 10.1038/nbt.1550.
61. Rinn, J.L., Kertesz, M., Wang, J.K., Squazzo, S.L., Xu, X., Brugmann, S.A., Goodnough, L.H., Helms, J.A., Farnham, P.J., Segal, E., and Chang, H.Y. (2007). Functional demarcation of active and silent chromatin domains in human HOX loci by noncoding RNAs. Cell *129*, 1311-1323. 10.1016/j.cell.2007.05.022.
62. Wu, L., Murat, P., Matak-Vinkovic, D., Murrell, A., and Balasubramanian, S. (2013). Binding interactions between long noncoding RNA HOTAIR and PRC2 proteins. Biochemistry *52*, 9519-9527. 10.1021/bi401085h.
63. Kuo, F.C., Neville, M.J., Sabaratnam, R., Wesolowska-Andersen, A., Phillips, D., Wittemans, L.B.L., van Dam, A.D., Loh, N.Y., Todorcevic, M., Denton, N., et al. (2022). HOTAIR interacts with PRC2 complex regulating the regional preadipocyte transcriptome and human fat distribution. Cell Rep *40*, 111136. 10.1016/j.celrep.2022.111136.
64. Dixon-McDougall, T., and Brown, C.J. (2021). Independent domains for recruitment of PRC1 and PRC2 by human XIST. PLoS Genet *17*, e1009123. 10.1371/journal.pgen.1009123.
65. Zovoilis, A., Cifuentes-Rojas, C., Chu, H.P., Hernandez, A.J., and Lee, J.T. (2016). Destabilization of B2 RNA by EZH2 Activates the Stress Response. Cell *167*, 1788-1802 e1713. 10.1016/j.cell.2016.11.041.
66. Cheng, Y., Saville, L., Gollen, B., Isaac, C., Belay, A., Mehla, J., Patel, K., Thakor, N., Mohajerani, M.H., and Zovoilis, A. (2020). Increased processing of SINE B2 ncRNAs unveils a novel type of transcriptome deregulation in amyloid beta neuropathology. Elife *9*. 10.7554/eLife.61265.
67. Cookis, T., Sauer, P., Poepsel, S., Han, B.G., Herbst, D.A., Glaeser, R., and Nogales, E. (2023). Streptavidin-Affinity Grid Fabrication for Cryo-Electron Microscopy Sample Preparation. J Vis Exp. 10.3791/66197.
68. Hafner, M., Katsantoni, M., Köster, T., Marks, J., Mukherjee, J., Staiger, D., Ule, J., and Zavolan, M. (2021). CLIP and complementary methods. Nature Reviews Methods Primers *1*, 20. 10.1038/s43586-021-00018-1.
69. Kundu, L.M., Linne, U., Marahiel, M., and Carell, T. (2004). RNA is more UV resistant than DNA: the formation of UV-induced DNA lesions is strongly sequence and conformation dependent. Chemistry *10*, 5697-5705. 10.1002/chem.200305731.
70. Laugesen, A., Hojfeldt, J.W., and Helin, K. (2019). Molecular Mechanisms Directing PRC2 Recruitment and H3K27 Methylation. Mol Cell *74*, 8-18. 10.1016/j.molcel.2019.03.011.
71. Hemphill, W.O., Fenske, R., Gooding, A.R., and Cech, T.R. (2023). PRC2 direct transfer from G-quadruplex RNA to dsDNA has implications for RNA-binding chromatin modifiers. Proc Natl Acad Sci U S A *120*, e2220528120. 10.1073/pnas.2220528120.

A

TERRA: 5' $(A)_{10}(GA)_4$**$(UUAGGG)_4$**$(AG)_4$ 3'

$TERRA_{mut}$: 5' $(A)_{10}(GA)_4$**$(UGAGUG)_4$**$(AG)_4$ 3'

pUG-fold: 5' $(A)_{10}$**$(GU)_{20}$** 3'

Poly(A): 5' $(A)_{10}$**$(A)_{40}$** 3'

B

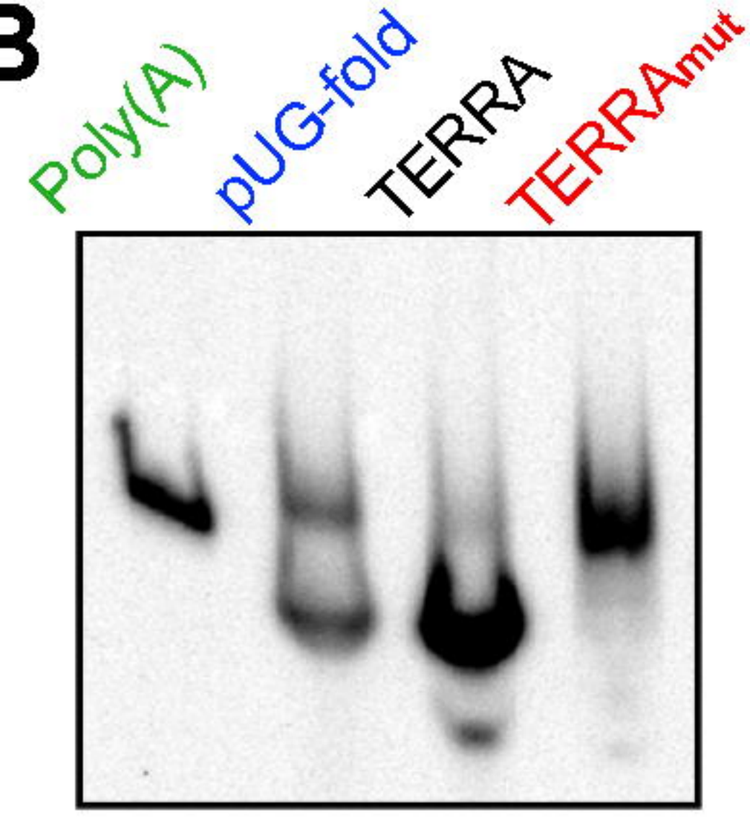

C

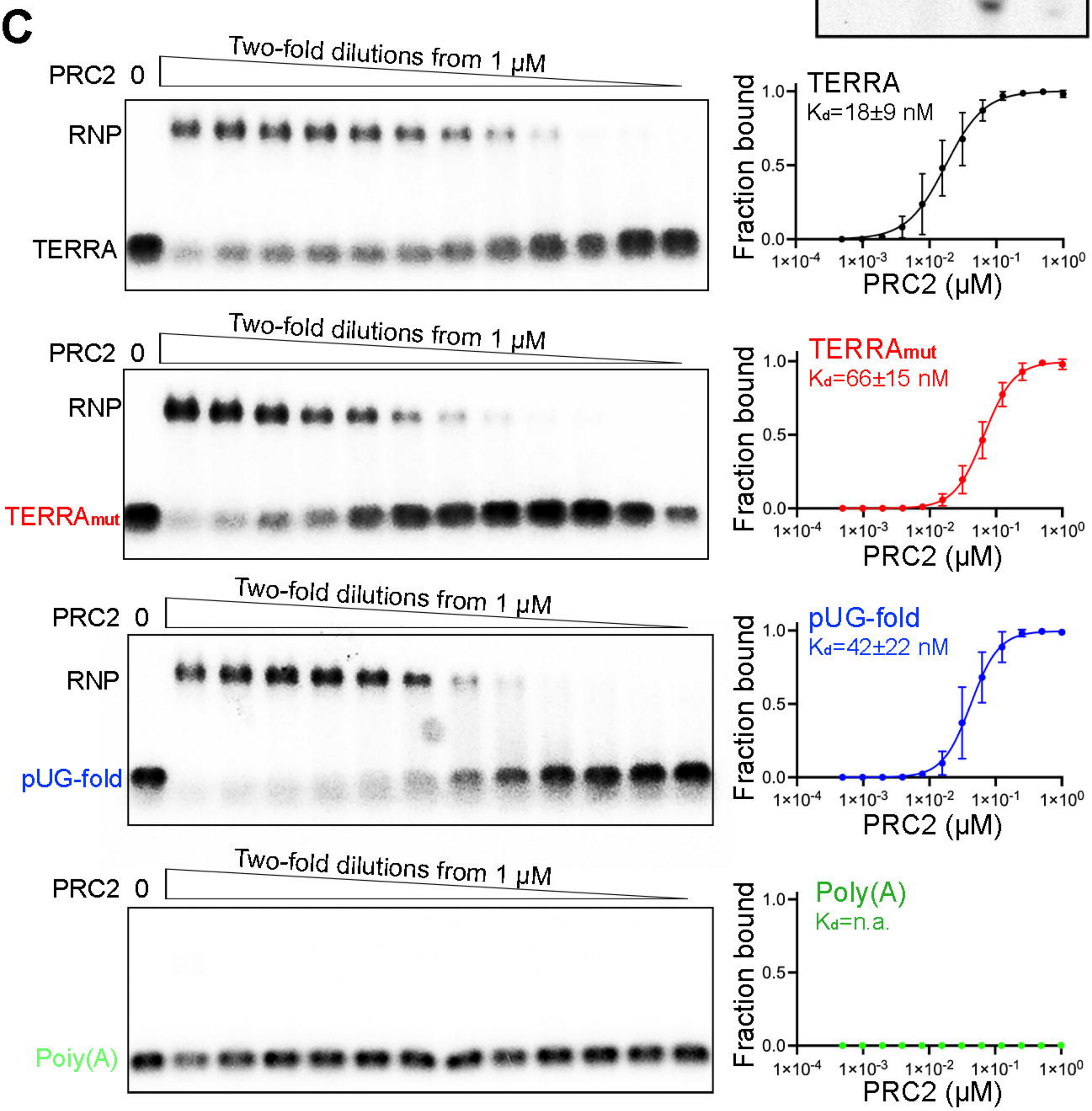

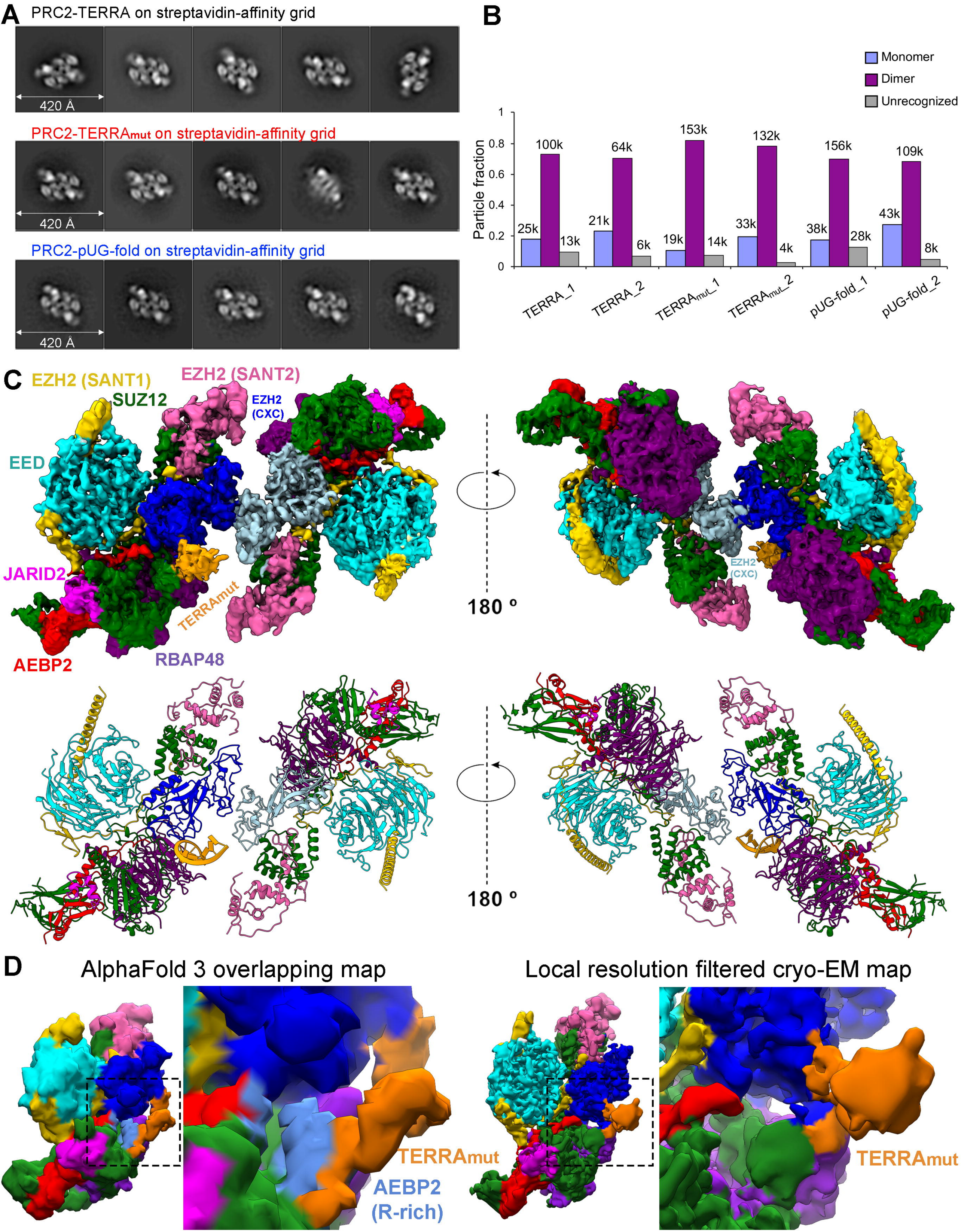
A
PRC2-TERRA on streptavidin-affinity grid
420 Å
PRC2-TERRAmut on streptavidin-affinity grid
420 Å
PRC2-pUG-fold on streptavidin-affinity grid
420 Å
B
Monomer
Dimer
Unrecognized
Particle fraction
1
0.8
0.6
0.4
0.2
0
25k
100k
13k
21k
64k
6k
19k
153k
14k
33k
132k
4k
38k
156k
28k
43k
109k
8k
TERRA_1
TERRA_2
TERRAmut_1
TERRAmut_2
pUG-fold_1
pUG-fold_2
C
EZH2 (SANT1)
EZH2 (SANT2)
SUZ12
EZH2 (CXC)
EED
JARID2
TERRAmut
AEBP2
RBAP48
180 °
EZH2 (CXC)
180 °
D
AlphaFold 3 overlapping map
Local resolution filtered cryo-EM map
TERRAmut
AEBP2 (R-rich)
TERRAmut

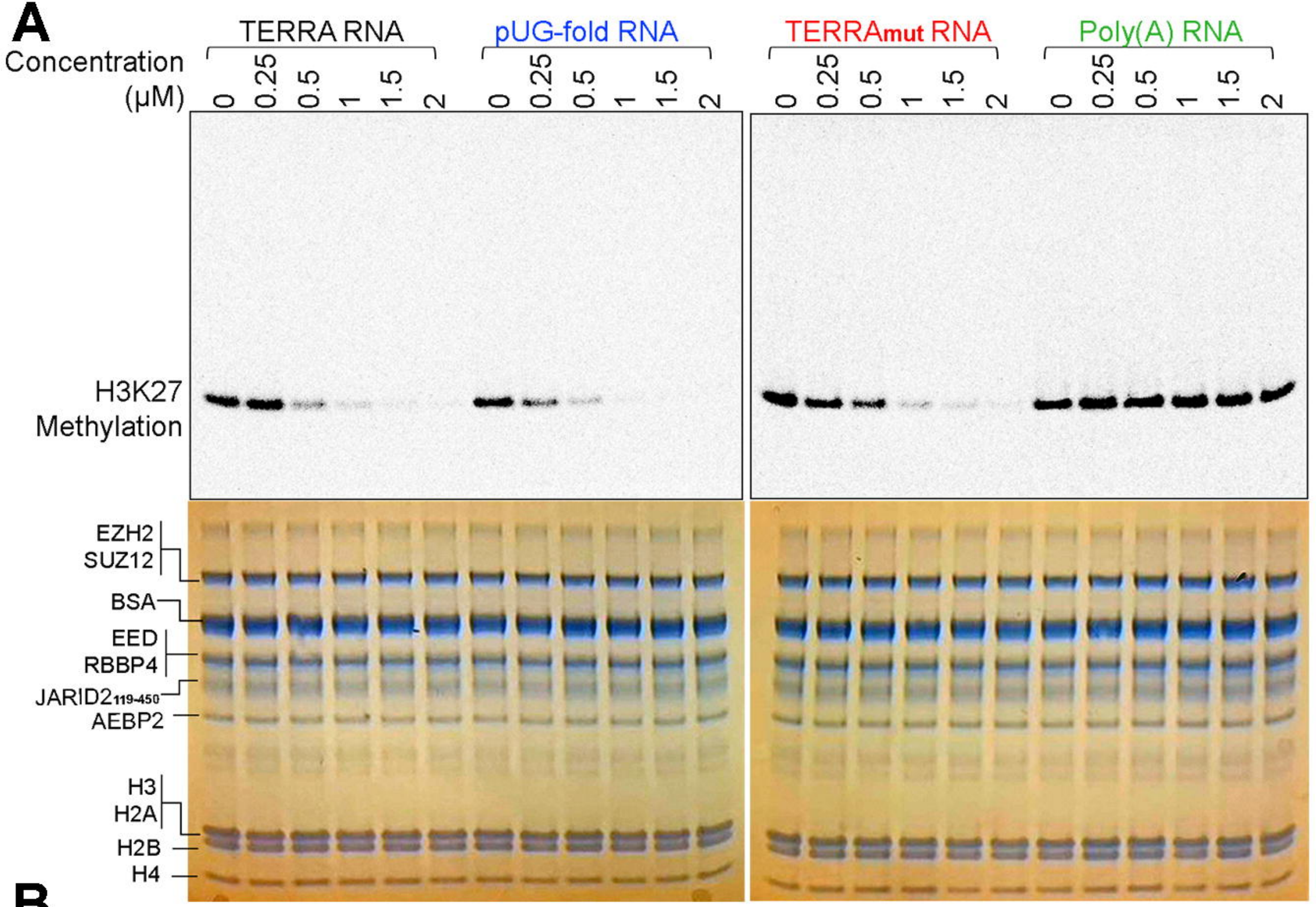
A
TERRA RNA
pUG-fold RNA
TERRAmut RNA
Poly(A) RNA
Concentration (μM)
0 0.25 0.5 1 1.5 2
H3K27 Methylation
EZH2
SUZ12
BSA
EED
RBBP4
JARID2119-450
AEBP2
H3
H2A
H2B
H4
B
Relative PRC2 activity
IC50=554±144 nM
TERRA RNA (nM)
IC50=442±11 nM
TERRAmut RNA (nM)
IC50=424±163 nM
pUG-fold RNA (nM)
IC50=n.a.
Poly(A) RNA (nM)
0.0
0.5
1.0
0
500
1000
1500
2000

A PTBP1-binding RNA: 5' $(UCUUUCU)_6$ 3'

2G4 RNA: 5' $(A)_{10}(GGGAA)_4(CAA)_5(GGGAA)_4$ 3'

B

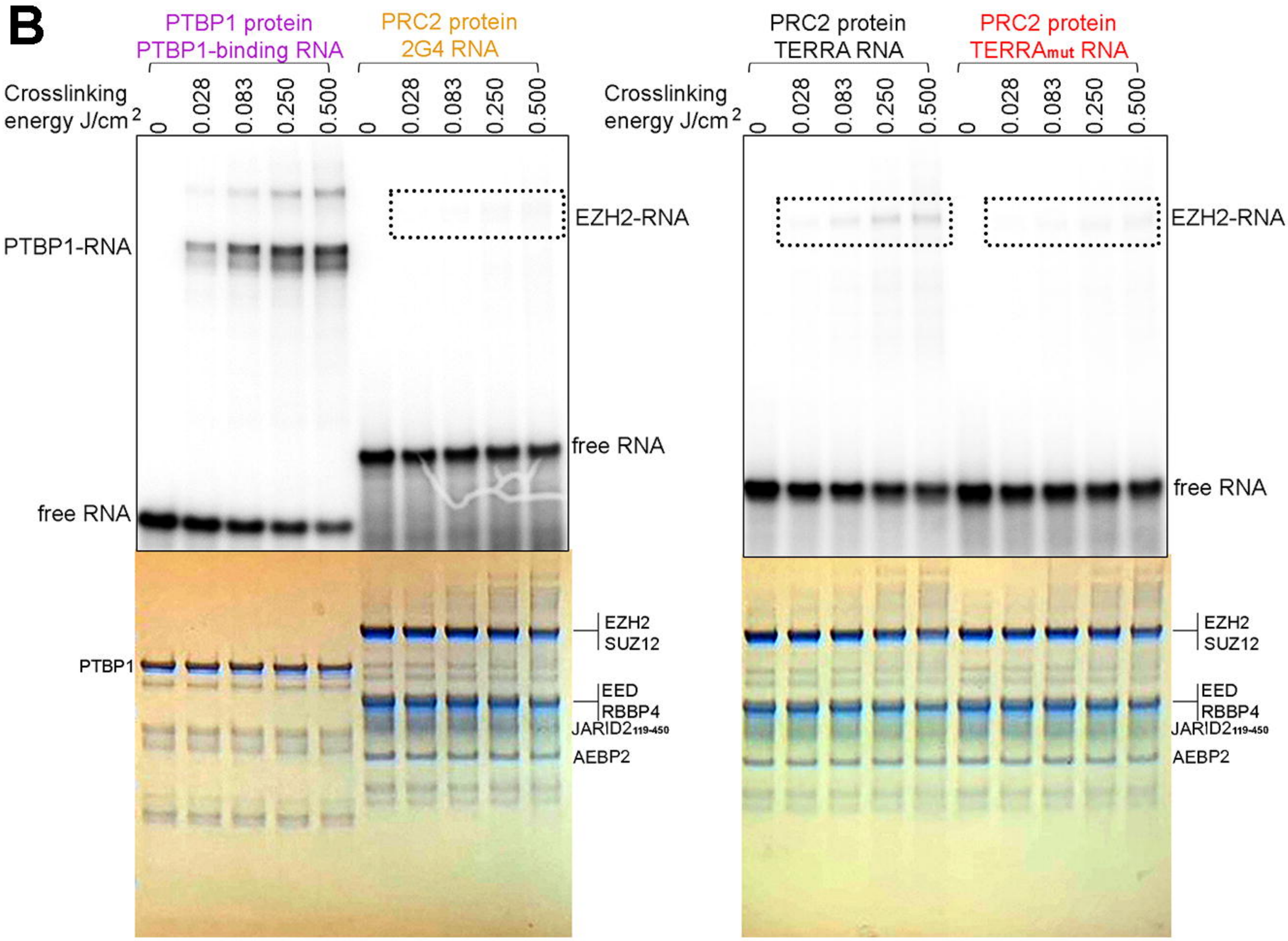
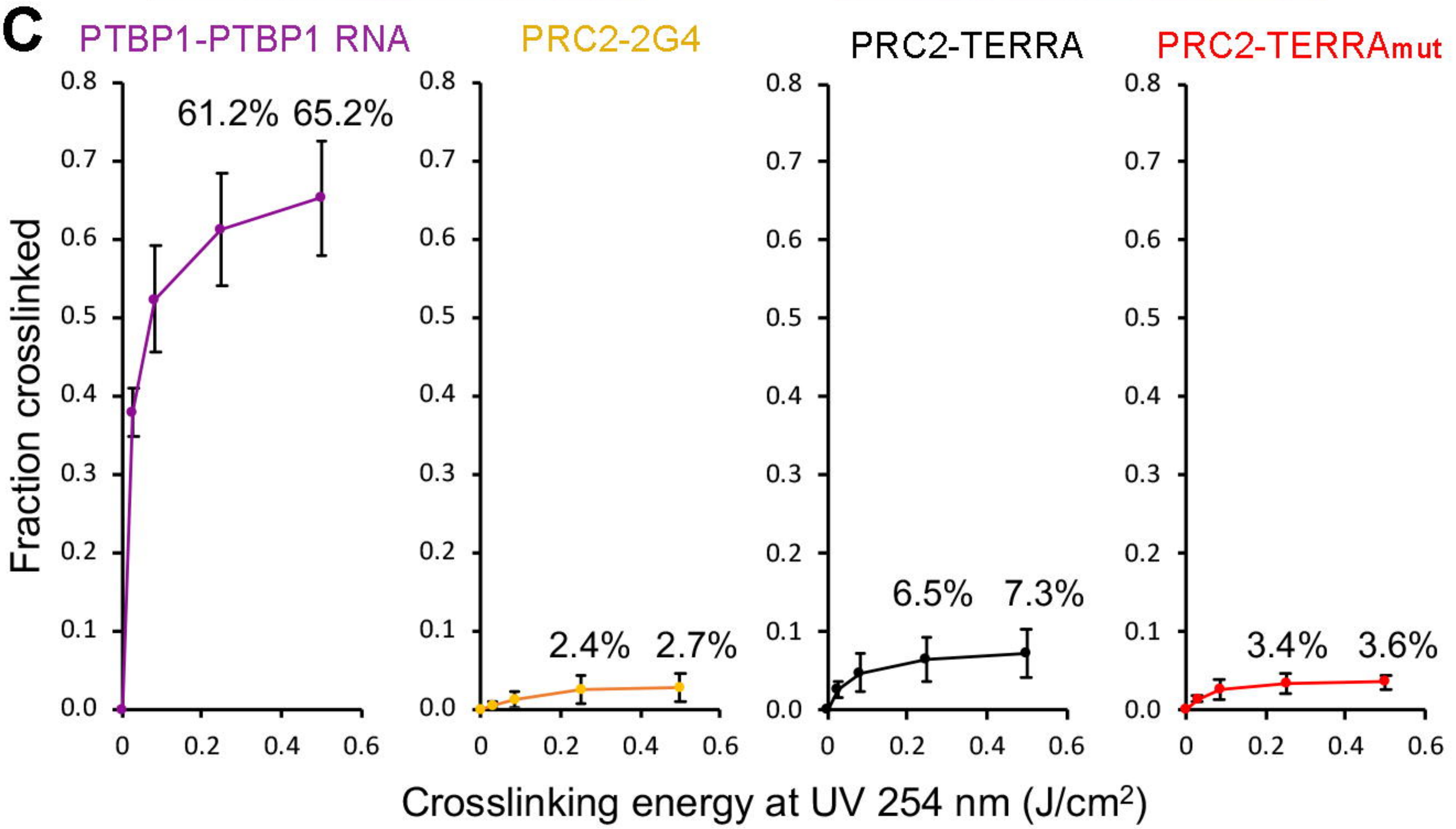
C